UC Berkeley
UC Berkeley Previously Published Works

Title

Model-based analysis of the impact of diffuse radiation on CO2 exchange in a temperate deciduous forest

Permalink

https://escholarship.org/uc/item/18b891wm

Authors

Lee, Min S
Hollinger, David Y
Keenan, Trevor F
et al.

Publication Date

2018-02-01

DOI

10.1016/j.agrformet.2017.11.016

Peer reviewed

eScholarship.org Powered by the California Digital Library
University of California

Model-based analysis of the impact of diffuse radiation on CO_2 exchange in a temperate deciduous forest

Min S.Lee[a] David Y.Hollinger[b] Trevor F. Keenan[c] Andrew P. Ouimette[d] Scott V. Ollinger[d] Andrew D. Richardson[aef]

Abstract

Clouds and aerosols increase the fraction of global solar irradiance that is diffuse light. This phenomenon is known to increase the photosynthetic light use efficiency (LUE) of closed-canopy vegetation by redistributing photosynthetic photon flux density (400–700 nm) from saturated, sunlit leaves at the top of the canopy, to shaded leaves deeper in the canopy. We combined a process-based carbon cycle model with 10 years of eddy covariance carbon flux measurements and other ancillary data sets to assess 1) how this LUE enhancement influences interannual variation in carbon uptake, and 2) how errors in modeling diffuse fraction affect predictions of carbon uptake. Modeled annual gross primary productivity (GPP) increased by ≈0.94% when observed levels of diffuse fraction were increased by 0.01 (holding total irradiance constant). The sensitivity of GPP to increases in diffuse fraction was highest when the diffuse fraction was low to begin with, and lowest when the diffuse fraction was already high. Diffuse fraction also explained significantly more of the interannual variability of modeled net ecosystem exchange (NEE), than did total irradiance. Two tested radiation partitioning models yielded over- and underestimates of diffuse fraction at our site, which propagated to over- and underestimates of annual NEE, respectively. Our findings highlight the importance of incorporating LUE enhancement under diffuse light into models of global primary production, and improving models of diffuse fraction.

Abbreviations:

f_d

diffuse fraction

PPFD

photosynthetic photon flux density

NEE

net ecosystem exchange

GPP

gross primary productivity

RE

ecosystem respiration

LUE

light use efficiency

Keywords

Diffuse radiation

Light use efficiency

Eddy covariance

Net ecosystem exchange

Deciduous forest

Canopy photosynthesis

1. Introduction

A key uncertainty of forest ecosystem carbon uptake in a changing climate is its differential responses to diffuse and direct beam solar radiation (Bonan, 2008; Heimann and Reichstein, 2008; Settele et al., 2014). Cloud cover and aerosols (Cheng et al., 2016; Niyogi et al., 2004) account for most of the variability in the ratio of diffuse to global irradiance (hereafter referred to as diffuse fraction), and projections of how these will change in the future are highly uncertain (Boucher et al., 2013; Wild, 2009). There is also uncertainty associated with the pathways through which diffuse fraction influences the carbon budget. Diffuse fraction affects the photosynthetic photon flux density (PPFD) distribution within the forest canopy, which has potentially important implications for canopy photosynthesis. Under clear sky conditions, sunlit leaves are often light saturated while shaded leaves receive little light and thus lie on the linear part of the light response curve (Roderick et al., 2001). Under diffuse light conditions, sunlit leaves receive less direct beam PPFD but shaded leaves receive more diffuse PPFD, which comes from all directions of the sky and penetrates the canopy to a fuller extent. Because leaves in deep shade benefit more from an increase in PPFD than leaves in full sun suffer from an equivalent decrease, a more even vertical distribution of PPFD should enhance the photosynthetic light use efficiency (LUE) of the canopy as a whole (Farquhar and Roderick, 2003). Direct measurements of forest CO_2 uptake have shown that canopy LUE is indeed enhanced under cloudy conditions, though estimates of enhancement vary (Alton, 2008; Alton et al., 2007; Baldocchi, 1997; Gu et al., 2002; Hollinger et al., 1994; Jenkins et al., 2007; Urban et al., 2007; Zhang et al., 2010). A number of studies have also found that aerosol loading events, such as the eruption of Mount Pinatubo (Farquhar and Roderick, 2003; Gu et al., 2003; Mercado et al., 2009), have enhanced the terrestrial carbon sink. However, aside from these studies of dramatic increases in diffuse fraction, there has been relatively little research on the extent to which interannual variation in diffuse fraction − typically stemming from fluctuations in cloudiness − mediates the interannual variation in carbon budget. Min and Wang (2008) find that the transmittance index, compared to temperature and precipitation, is more highly correlated ($R^2 > 0.65$) with mean midsummer net ecosystem

production at a northern hardwood forest, which suggests LUE changes with cloudiness may accumulate over the growing season in annually distinct ways and have meaningful influence on forest productivity in a given year.

Diffuse fraction also covaries with other environmental factors that impact the carbon budget. The presence of clouds and aerosols often reduces the solar radiation reaching Earth's surface, and is associated with lower air and leaf temperature and vapor pressuredeficit (Gu et al., 2002; Oliphant et al., 2011; Wohlfahrt et al., 2008; Zhang et al., 2011). Less incident PPFD reduces photosynthesis, while the thermal effects can enhance photosynthesis when ambient temperature is above the optimum (Baldocchi and Harley, 1995; Steiner and Chameides, 2005) and reduce ecosystem respiration (Alton, 2008; Gu et al., 1999; Urban et al., 2007). Lower vapor pressure deficit (VPD) associated with reduced irradiance can increase stomatal conductance, enhancing leaf photosynthesis (Gu et al., 1999). Recent studies suggest the decrease in total irradiance has a greater effect on the net ecosystem exchange (NEE) than associated changes in temperature and humidity (Alton et al., 2007; Knohl and Baldocchi, 2008; Oliphant et al., 2011), though quantifying these separately remains difficult (Kanniah et al., 2012).

In this paper, we investigated the impacts of diffuse radiation on forest gross primary productivity (GPP) by combining long-term data sets (half-hourly measurements over 10 years) of eddy covariance fluxes and direct and diffuse PPFD with a process-oriented model. Many studies have estimated diffuse fraction using radiation partitioning models (Alton, 2008; Alton et al., 2007; Choudhury, 2001; Gu et al., 2002; Rocha et al., 2004). The performance of these radiation partitioning models can vary with site (Boland et al., 2001; Schurgers et al., 2015) due to differences in geographic or climatic factors like cloud cover and type, sunshine duration, and particulate matter in the air (Cruse et al., 2015). Studies using observed diffuse fraction have typically relied on records of a few years or less (Gu et al., 2002; Hollinger et al., 1994; Jenkins et al., 2007; Niyogi et al., 2004; but see Cheng et al., 2015), which may not adequately capture the variability of NEE responses to diffuse fraction and other meteorological drivers. Our analysis also allowed us to account for additional factors that affect ecosystem productivity, including temperature, VPD, and total irradiance. These variables interact with GPP through multiple pathways (e.g., air temperature influences photosynthetic rates as well as the growing period length) and lagged effects (e.g., changes in leaf photosynthesis affect GPP, which, in turn, can affect carbon allocation to foliage), which are difficult to quantify using a purely empirical model. The parameters of our forest carbon cycle model were optimized against multiple observational data constraints, allowing us to explicitly isolate the impact of diffuse fraction on the distribution of light in the canopy (and hence on GPP).

Next, we examined the extent to which interannual variability of diffuse fraction mediates the interannual variability of modeled NEE. Studies have

often asked whether and when increasing diffuse fraction poses a productivity trade-off between total irradiance and LUE; a common finding is that diffuse fraction above a certain threshold causes net decrease in NEE because the accompanying reductions in incident PPFD outweigh improvements in LUE (Alton, 2008; Knohl and Baldocchi, 2008; Mercado et al., 2009; Oliveira et al., 2007; Still et al., 2009). We asked a related but different question: how much does variability of diffuse fraction influence the modeled NEE of a given year, compared to variability of total PPFD? Answering this question provides insights into the relative importance of diffuse fraction for accurately modeling carbon budgets at longer time scales.

Finally, we tested the accuracy of two standard partitioning models used to predict diffuse fraction, and analyzed the impact of their errors on predictions of NEE and other carbon cycle components. While studies have measured the goodness of fit between observations and predictions of NEE that were informed by modeled diffuse fraction (Gu et al., 2002; Rocha et al., 2004; Schurgers et al., 2015), and Gu et al. (2002) compare independently parameterized models utilizing observed and modeled diffuse fraction, this is the first study to our knowledge that has compared performances of model runs differing only in the accuracy of their diffuse and direct PPFD drivers. Our findings help gauge the importance of improving diffuse fraction models to better replicate forest carbon dynamics.

To achieve these three objectives, we first optimized and validated a process-based model using 10 years of half-hourly eddy covariance fluxes, observations of direct and diffuse PPFD, and other ancillary measurements at the Bartlett Experimental Forest, a deciduous site in the northeastern United States. After optimizing model parameters using the first half of our observational record, and validating the model against the second half, we then prescribed various scenarios of diffuse fraction to measure how model outputs and performance respond.

2. Materials and methods

2.1. Site

The Bartlett Experimental Forest (BEF) (https://www.nrs.fs.fed.us/ef/locations/nh/bartlett/) is a primarily deciduous forest located in the northeastern United States (44.05° N, 71.29° W). Mean annual temperature is approximately 6.6°C (summer: 20°C, winter: −8°C), and mean annual precipitation is approximately 1300 mm, distributed evenly throughout the year. The soils are Spodosols, developed on glacial till derived from granite and gneiss. Soils are well drained, acidic, and nutrient poor.

Forest stands around the tower are generally 90–130 y in age, dominated by the deciduous species *Acer rubrum* (red maple) and *Fagus grandifolia* (American beech), with lesser amounts of Acer *saccharum* (sugar

maple), Betula papyrifera (paper birch) and *Betula alleghaniensis* (yellow birch). Conifers like *Tsuga* canadensis (eastern hemlock), *Abies balsamea* (balsam fir), and *Pinus* strobus (Eastern white pine) are present around the tower in smaller numbers compared to the deciduous species.

2.2. Data

We combined ten years (2004-13) of half-hourly NEE flux measurements with ancillary data sets—soil respiration, wood growth, foliar and woody litterfall, leaf area index, turnover times of litter and soil organic matter pools—to train and validate our model (Table 1). Data from the first five years (2004-08) were used for training, data from the last five years (2009-13) for validation. We prescribed meteorological drivers in each period at half-hourly intervals in line with the model structure (see Section 2.3.1).

Table 1. Data used to constrain the model. The training period consists of years 2004-08, and the validation period consists of years 2009-13. For litter and soil carbon turnover, the same turnover time was used during training and validation periods.

Measurement	**Frequency**	**Number of Data Points**	
		Training	**Validation**
Eddy-covariance	Half-hourly	24,312	24,887
Soil respiration	Daily	75	0
Wood growth	Yearly	4	5
Foliar litterfall	Yearly	5	2
Woody litterfall	Yearly	2	0
Leaf area index	Yearly	3	0
Litter turnover	One	1	
Soil carbon turnover (microbial)	One	1	
Soil carbon turnover (slow)	One	1	
Soil carbon turnover (passive)	One	1	

NEE and meteorological measurements were obtained from the Bartlett AmeriFlux tower (http://ameriflux.lbl.gov/sites/siteinfo/US-Bar). NEE was measured with the eddy covariancetechnique (Foken et al., 2012) using a model SAT-211/3 K three-axis sonic anemometer(Applied Technologies Inc., Longmont, CO) and a model LI-6262 fast response CO_2/H_2O infrared gas analyzer (Li-Cor Inc., Lincoln, NE), with data recorded at 5 Hz and fluxes (covariances) calculated every 30 min. Instrument configuration, calibration protocol, QA/QC and data processing procedures are identical to those used at the Howland AmeriFlux site in central Maine, and are documented by Hollinger et al. (2004). We removed nighttime NEE values with friction velocity (u*) below 0.50, a threshold derived from the change-point model in Barr et al. (2013). We trained the model on NEE measurements, and used gap-filled NEE only to assess optimized model performance at annual and monthly time scales. Meteorological measurements were recorded every 5 s and half-hourly means stored on data loggers (models CR10 and CR21x; Campbell Scientific, Logan UT). These included air temperature and relative humidity above the canopy (HMP-35, Vaisala Inc.), soil temperatureat 5 cm (thermocouple), and direct and diffuse PPFD (BF3 Sunshine Sensor, Delta-T Devices Ltd., Cambridge UK). Measurements of direct and diffuse PPFD began on June 10 of 2004, the first year of the training period. For days prior to June 10 of 2004, direct and diffuse PPFD were estimated using the model in Spitters et al. (1986) (see Section 2.3.3).

All ancillary data used to constrain the model, except turnover times of litter and soil pools, were obtained from the Earth Systems Research Center at the University of New Hampshire (Bradford et al., 2010). These measurements were taken in 12 plots within the 1 km^2footprint of the Bartlett tower, each divided into four sub-plots, as described by Hollinger (2008). Soil respiration was measured about every three weeks during the snow-free portion of the year (3424 measurements over 75 days during 2004-07) using a model LI-820 infrared gas analyzer (Li-Cor Inc., Lincoln, NE) and three 10 inch PVC collars per sub-plot: collar concentrations of CO_2 were measured every 2 s over a 60 s period, and the rate of change of concentration was converted to flux. We constrained the model against mean soil respiration flux over the course of the day. For wood growth, diameter at breast height was measured to calculate basal area of trees, which was converted to biomass using allometric equations by Hocker and Earley (1983), Whittaker et al. (1974), and Young et al. (1980). To account for uncertainties associated with diameter measurements, carbon concentration in the wood, and choice of allometric model, a Monte Carlo simulation was used to estimate annual wood growth (g C m^{-2} yr^{-1}), similar to Yanai et al. (2010). Mean of 1000 iterations was calculated for each plot and then averaged across plots to yield a single estimate of wood growth per year. Foliar and woody litterfall were collected using two baskets per sub-plot, three times in autumn and once in spring. Annual litterfall was calculated by summing the weight of litter for the year and dividing by area of the baskets, and then converted to

biomass (g C m^{-2} yr^{-1}) by assuming carbon concentration of 49% (Bernier et al., 2008). Leaf area index (LAI) was measured annually in sub-plots using the LAI-2000 Plant Canopy Analyzer (Li-Cor Inc, Lincoln NE). Finally, we obtained turnover times of litter and the three soil organic matter pools (microbial, slow, passive) from McFarlane et al. (2013). We assumed that the microbial pool corresponds to the Oi soil layer, the slow pool to the Oe and Oa soil layers, and the passive pool to the 0–30 cm mineral soil layer.

We estimated uncertainties for each data stream used to constrain the model. Uncertainties of half-hourly NEE fluxes were calculated as shown in Richardson et al. (2006), where uncertainties follow a double-exponential distribution, the standard deviation of which scales linearly with the flux magnitude. For gap-filled NEE totals, we accounted for measurement, gap-filling, and friction velocity (u*) uncertainties following the approach of Barr et al. (2013). Uncertainties for mean soil respiration flux were estimated as standard deviations of the fluxes averaged over the day. Uncertainties for annual wood growth were first estimated for each plot using the 95% confidence intervals of 1000 Monte Carlo simulation iterations, and then propagated with spatial variability. Uncertainties for foliar and woody litterfall were estimated as sampling errors (standard errors of mean values across all plots). LAIuncertainties were estimated as sums of standard errors and instrument errors (±0.1). We obtained uncertainties for turnover times and initial carbon stocks of soil pools from McFarlane et al. (2013).

2.3. Model structures

2.3.1. FöBAAR

We used a forest carbon cycle model called Forest Biomass, Assimilation, Allocation, and Respiration (FöBAAR), developed by Keenan et al. (2012), which runs on a half-hourly time step with 37 free parameters (Table 2). FöBAAR uses Norman's (1982) canopy model to calculate photosynthetic photon flux density (PPFD) for two leaf classes (shaded and sunlit), based on direct and diffuse PPFD. Photosynthesis is modeled as a function of PPFD, air temperature, VPD, and intercellular concentration of CO_2 using a Farquhar-type approach (De Pury and Farquhar, 1997; Farquhar et al., 1980). The net rate of leaf photosynthesis equals the gross rate of photosynthesis minus the leaf respiration rate, where the gross rate is calculated as the minimum of electron-transport limited photosynthesis and Rubisco-limited photosynthesis. Electron-transport limited photosynthesis is a function of the electron transport rate per unit leaf area, intercellular concentration of CO_2, and CO_2 compensation point of photosynthesis. Rubisco-limited photosynthesis depends on the maximum Rubisco rate, intercellular concentrations of CO_2 and O_2, temperature-dependent Michaelis-Menten constants for CO_2 and O_2, and the CO_2 compensation point (De Pury and Farquhar, 1997). The intercellular concentration of O_2 is fixed at 21%. The ratio of the maximum electron transport rate (J_{max}) to the maximum Rubisco rate (Vc_{max}) is assumed to be fixed at 2.1 at 298 K (Wullschleger,

1993), and the temperature dependencies of J_{max} and Vc_{max} are modeled with Arrhenius functions (De Pury and Farquhar, 1997). Arrhenius-type equations are also used to calculate the CO_2 compensation point and mitochondrial respiration rate (Bernacchi et al., 2001). Stomatal conductance, calculated using the Ball-Berry model (Ball et al., 1987), is coupled to the net rate of leaf photosynthesis through an analytical solution (Baldocchi, 1994). Rates of photosynthesis for the two leaf classes are integrated over their respective LAIs, and the sum of these two results is integrated over time to calculate canopy productivity over a period.

Table 2. FöBAAR model parameters and pools. “Min” and “Max” indicate the range of parameter values explored during optimization. “90% CI” gives the range of parameter values accepted after posterior chi-squared tests at 90% confidence for the model run that was optimized to all data constraints with observed diffuse fraction.

Id	Name	Definition	Min	Max	90% CI
			Initial carbon pools ($g\ C\ m^{-2}$)		
P1	R_c	Carbon in roots	30	500	369, 378
P2	W_c	Carbon in wood	10300	10508	10300, 10508
P3	Lit_c	Carbon in litter	10	1000	435, 484
P4	SOM_M	Carbon in microbial soil organic matter pool	183	193	183, 185
P5	SOM_S	Carbon in slow soil organic matter pool	3186	3356	3210, 3356
P6	SOM_P	Carbon in passive soil organic matter pool	8129	8564	8130, 8424
P7	Mob_c	Mobile carbon	50	500	345, 406
			Allocation and transfer		
P8	A_f	Fraction of GPP allocated to foliage	0.1	1	0.72, 0.80
P9	A_r	Fraction of NPP allocated to	0.1	1	0.80,

Id	Name	Definition	Min	Max	90% CI
		roots			0.82
P10	Lf_f	Litterfall from foliage (Log_{10})	−6	−0.5	−1.20, −1.11
P11	Lf_w	Litterfall from wood (Log_{10})	−6	−1	−5.22, −4.95
P12	Lf_r	Litterfall from roots (Log_{10})	−6	−1	−5.49, −5.15
P13	Fc_lf	Fraction of foliage carbon not transferred to mobile carbon	0.1	1	0.81, 0.84
P14	$LitSOM_M$	Litter to microbial SOM transfer rate (Log_{10})	−8	−1	−6.91,−6.05
P15	SOM_MSOM_S	Microbial SOM to slow SOM rate	0.01	0.95	0.68, 0.92
P16	SOM_SSOM_P	Slow SOM to passive SOM rate	0.01	0.95	0.44, 0.89
			Canopy		
P17	LMA	Leaf mass per area (g C m^{-2})	25	30	29, 30
P18	Vc_{max}	Maximum Rubisco rate at 25°C (µmol $m^{-2}s^{-1}$)	50	175	62, 68
P19	g_sD_0	Coefficient in Ball-Berry-Leuning model	0.95	4.5	3.92, 4.23
P20	θ_1	Curvature of leaf response of electron transport to irradiance	0.3	0.9	0.34,0.36
P21	Rd	Rate of dark respiration	0.01	0.9	0.02, 0.03
P22	Q10 Rd	Temperature dependence of Rd	0.5	2.5	0.70, 0.71

Id	Name	Definition	Min	Max	90% CI
			Phenology		
P23	GDD_0	Day of year for growing degree day start	50	150	80, 82
P24	GDD_1	Growing degree days for spring onset	100	500	221, 229
P25	Air T_S	Leaf senescence onset mean air temperature	1	25	8.7, 9.1
P26	GDD_2	Spring photosynthetic GDD maximum	30	1000	71.6, 93.1
P27	Fol_g	Duration of leaf growth	15	90	47, 49
			Respiration		
P28	RLit	Litter respiration rate (Log_{10})	−8	−1	−4.8, −4.5
P29	$RLitT_d$	Litter respiration temperature dependence	0.001	0.2	0.01, 0.02
P30	$RSOM_M$	Microbial SOM respiration rate (Log_{10})	−8	−1	−5.6, −5.4
P31	$RSOM_S$	Slow SOM respiration rate (Log_{10})	−8	−1	−6.7, −6.2
P32	$RSOM_P$	Passive SOM respiration rate (Log_{10})	−8	−1	−7.3, −7.0
P33	RMob	Mobile stored carbon respiration rate (Log_{10})	−6	−0.5	−2.9, −2.8
P34	$RSOMT_d$	SOM respiration temperature dependence	0.001	0.2	0.07, 0.1
P35	Rroot	Root respiration rate (Log_{10})	−7	−1	−4.3, −4.1
P3	$RootT_d$	Root respiration temperature	0.001	0.3	0.1, 0.2

Id	Name	Definition	Min	Max	90% CI
6		dependence			
P37	$GPPF_r$	Fraction of GPP respired for maintenance	0.1	0.5	0.3, 0.4

A percentage of the assimilated carbon is respired daily, and the rest is distributed among foliage, wood, and roots. Root respiration depends on the allocated carbon and soil temperature. Budburst and senescence are determined using growing degree day (GDD) formulas. Litterfall decomposes and then is passed through three progressively more recalcitrant soil organic matter (SOM) pools: microbial, slow, and passive. Heterotrophic respiration from the litter and SOM pools occurs as a function of a base rate parameter and a temperature sensitivity parameter.

2.3.2. Canopy radiation model

The Norman (1982) sun-shade canopy model was used to translate direct and diffuse PPFD into PPFD on shaded and sunlit leaves. The PPFD on shaded leaves, I_{shade}, is the sum of diffuse PPFD and scattered direct beam:

$$I_{\text{shade}} = I_{\text{dif}}\mathrm{e}^{(-0.5F^{0.7})} + C \quad (1)$$

where I_{dif} is the diffuse PPFD on a horizontal plane above the canopy, F is the total LAI, and C is the direct beam scattered by the canopy. The exponential term represents the extinction of the diffuse component. Norman (1982) expresses the scattered direct beam, C as:

$$C = \mathrm{kI}_{\text{dir}}(1.1\text{-}0.1F)\mathrm{e}^{-\sin(\theta)} \quad (2)$$

where k is the scattering coefficient set at 0.07, I_{dir} is the direct PPFD on a horizontal plane above the canopy, and θ is the solar elevation angle. Scattered direct beam decreases as canopy depth or solar elevation angle increases. The PPFD on sunlit leaves, I_{sun}, is calculated as:

$$I_{\text{sun}} = \frac{I_{\text{dir}}\cos(a)}{\sin(\theta)} + I_{\text{shade}} \quad (3)$$

where a is the mean leaf-sun angle. We assume a equals 60° for a spherical leaf angle distribution (Goudriaan, 1988). I_{shade} and I_{sun} are used to calculate photosynthesis per leaf area for shaded and sunlit leaves, which are then multiplied by the shaded and sunlit LAIs, respectively, to compute GPP from shaded and sunlit leaves. The sunlit LAI is F_{sun} and the shaded LAI is F_{shade} as follows:

$$F_{sun} = \left(1 - \mathrm{e}^{\frac{-0.5F}{\sin(\theta)}}\right) 2\sin(\theta) \quad (4)$$

$$F_{\mathrm{shade}} = F\text{-}F_{\mathrm{sun}} \quad (5)$$

The sum of GPP from shaded and sunlit leaves gives the total GPP.

2.3.3. Diffuse fraction models

For our final experiment, we incorporated models for estimating diffuse fraction of incoming PPFD from Weiss and Norman (1985) and Spitters et al. (1986). Both models have been widely used for carbon cycle modeling (Reed et al., 2014, Knorr and Kattge, 2005, Mercado et al., 2006) and other applications (Bash et al., 2016; Cabrera-Bosquet et al., 2016; Fleisher et al., 2015), though comparisons of their performance against observations are relatively sparse (see Schurgers et al., 2015 for assessment of the Spitters et al. model).

The Weiss and Norman model first calculates potential visible radiation on the horizontal plane for direct (R_{DV}) and diffuse (R_{dV}) components as follows:

$$R_{\mathrm{DV}} = \left(600\ \mathrm{e}^{-0.185m(P/P_0)}\right)\sin(\theta) \quad (6)$$

$$R_{\mathrm{dV}} = 0.4(600 - R_{DV})\sin(\theta) \quad (7)$$

where m is optical air mass, P/P_0 the ratio of actual to sea level pressure, and θ the solar elevation angle. We estimated P/P_0 to be ≈0.97 using the barometric formula. Air mass m is a function of θ*:*

$$m = (\cos\ \theta)^{-1} \quad (8)$$

Total potential visible radiation on the horizontal plane, R_V, is just the sum of potential direct and diffuse components:

$$R_V = R_{\mathrm{DV}} + R_{\mathrm{dV}} \quad (9)$$

Next, the Weiss and Norman model calculates potential direct (R_{DN}) and diffuse (R_{dN}) components of near-infrared radiation (NIR):

$$R_{DN} = \left(720\, \mathrm{e}^{-0.06m(P/P_0)} - w\right)\sin(\theta) \quad (10)$$

$$R_{\mathrm{dN}} = 0.6(720 - R_{DN} - w)\sin(\theta) \quad (11)$$

where w is the water absorption in the near-infrared for 10 mm of precipitable water:

$$w = 1320 * 10^{\left[-1.1950+0.4459\log_{10} m-0.0345(\log_{10} m)^2\right]} \quad (12)$$

Total potential NIR on the horizontal plane, R_N, is again the sum of its direct and diffuse components:

$$R_N = R_{\mathrm{DN}} + R_{\mathrm{dN}} \quad (13)$$

Fraction of incident visible radiation that is direct (f_D) and diffuse (f_d) is then estimated as:

$$f_D = \frac{R_{DV}}{R_V}\left(1 - \left[\frac{0.9 - \frac{R_T}{R_V + R_N}}{0.7}\right]^{2/3}\right) \quad (14)$$

$$f_d = 1\text{-}f_D \quad (15)$$

where R_T is observed incoming solar radiation (visible and NIR). Therefore, the higher the share of direct component in potential visible radiation, the higher the predicted share of the direct component in observed visible radiation. f_D also increases with the ratio of observed to potential radiation.

The Spitters et al. model (1986) estimates diffuse fraction (f_d) as a function of atmospheric transmissivity (S_g/S_o):

$$f_d = \begin{cases} 1 & S_g/S_o \le 0.22 \\ 1 - 6.4(S_g/S_o - 0.22)^2 & 0.22 < S_g/S_o \le 0.35 \\ 1.47 - 1.66(S_g/S_o) & 0.35 < S_g/S_o \le K \\ R & K < S_g/S_o \end{cases} \quad (16)$$

where S_g and S_o are global and extra-terrestrial irradiance respectively, $R = 0.847–1.61 \sin(\theta) + 1.04 \sin^2(\theta)$,

and K = (1.47–R)/1.66. Extra-terrestrial irradiance at a plane parallel to Earth's surface, S_o, is estimated as:

$$S_o = 1370\{1+0.033\cos(360t_d/365)\}\sin(\theta) \quad (17)$$

where t_d is day number of the year.

2.4. Model optimization

We used a Markov Chain Monte Carlo (MCMC) algorithm to optimize the model against data constraints and to explore the posterior distribution of optimized parameters. The algorithm utilizes the Metropolis-Hastings method (Hastings, 1970; Metropolis et al., 1953) with simulated annealing (Press et al., 2007). Simulated annealing is a widely used technique that likens the search for minimum cost function value to the cooling of liquid material into a state of minimum energy, where temperatures start high to allow the algorithm to accept solutions that are worse than the current best (to escape any local optima), and gradually cool to focus the search on a global optimum. At each iteration of the optimization, the model steps from one parameter set to another, the size of the step being a randomly sampled fraction of the prior parameter range and a function of the annealing temperature. The step size also adjusts to yield an acceptance rate of ~20%, which we have found leads to efficient posterior exploration and well-performing parameter sets. We assume uniform prior distributions of parameters.

The first phase of optimization entails searching the parameter space for 120,000 iterations to achieve the minimum value for the aggregate cost function, which calculates the model-data mismatch across all data streams used to constrain the model. As in Keenan et al. (2011), each data stream has a normalized root mean squared error (NRMSE), or uncertainty-weighted square of the model error, averaged across the number of observations:

$$\mathrm{NRMSE}_i = \left(\sum_{t=1}^{N_i}\left(\frac{O_i(t)\text{-}M_i(t)}{\delta_i(t)}\right)^2\right)/N_i \quad (18)$$

where N_i is the number of observations for data stream i, $O_i(t)$ is the observation at time t, $M_i(t)$ is the modeled value for the same time, and $\delta_i(t)$ is the uncertainty of the observation. The aggregate cost function J is then the mean of all NRMSEs:

$$J = \left(\sum_{i=1}^{Q}\mathrm{NRMSE}_i\right)/Q \quad (19)$$

where Q is the number of data constraints. By giving equal weight to each data stream, the aggregate cost function favors balanced model

performance that accurately represents various ecosystem processes (Barrett et al., 2005; Franks et al., 1999).

The second phase of optimization involves identifying parameter sets consistent with the optimal set found in the first phase. A parameter set is accepted only if the NRMSE for each data stream passes the chi-square test at 90% confidence, where the critical values are determined from the optimal parameter set. This way, model performance is comparable across data streams (Richardson et al., 2010). We used 1000 accepted parameter sets to generate the posterior distributions in Table 2.

2.5. Experimental set-up

We first constructed a base scenario against which later model runs with different diffuse fraction settings could be compared. In this base scenario, we optimized the model to half-hourly, monthly, and yearly NEE data and the full suite of ancillary measurements, feeding in observed diffuse fraction alongside other meteorological drivers. Data from the first five years (2004-08) were used for optimization, and the latter five years (2009-13) for validation of optimized performance. We examined how accurately FöBAAR predicted NEE in each period when utilizing all available information at the study site.

We then conducted three experiments to assess how changes in diffuse fraction impact FöBAAR outputs and performance. In Experiment (1), we ran the model using the optimal parameter set from the base scenario but under five different scenarios of diffuse fraction (f_d): (1) all PPFD is direct ($f_d = 0$) (2) all PPFD is diffuse ($f_d = 1$) (3) PPFD is equal parts direct and diffuse ($f_d = 0.5$) (4) f_d is 0.01 higher than observed (5) f_d is 0.01 lower than observed. Total PPFD was kept at observed values across the scenarios. We compared how PPFD and GPP change for shaded and sunlit leaves in Scenarios (1) − (3), given the structure of Norman's canopy model. We used Scenarios (4) and (5) to assess GPP's sensitivity to small changes in diffuse radiation (±1 percentage point change in percentage of diffuse radiation).

In Experiment (2), we again used the same parameter set as before but prescribed two scenarios in which either f_d or PPFD deviates from observations: (1) every half-hour of the year is assigned observed PPFD but mean time-varying f_d (mean observed f_d for that half-hour across all years, see Table 3 for an example) (2) every half-hour is assigned observed f_d but mean time-varying PPFD. We compared the annual NEE of these two model runs with that from the base scenario to understand the relative impact of interannual variation in f_d on the modeled interannual carbon budgets.

Table 3. Summary of experiments and scenarios, with illustration of how a hypothetical base scenario would be altered under each experiment and scenario. For all but Experiment 2, Scenario 2, the photosynthetic photon flux density (PPFD) remains constant at observed values while diffuse fraction (f_d) is changed from observed values. Note that only one half-hour of

three years is shown here for simplicity, but all half-hours of all ten years (2004-13) are affected in each experiment and scenario.

Experiments and Scenarios	**Hypothetical Example: 10:00–10:30 am of June 11**					
	2004		**2005**		**2006**	
	PPFD	**f_d**	**PPFD**	**f_d**	**PPFD**	**f_d**
Base Scenario (Observed values)	**1000**	**0.5**	**1500**	**0.3**	**500**	**0.7**
Experiment 1, Scenario 1 ($f_d = 0$)	1000	0	1500	0	500	0
Experiment 1, Scenario 2 ($f_d = 1$)	1000	1	1500	1	500	1
Experiment 1, Scenario 3 ($f_d = 0.5$)	1000	0.5	1500	0.5	500	0.5
Experiment 1, Scenario 4 ($f_d = f_d + 0.01$)	1000	0.51	1500	0.31	500	0.71
Experiment 1, Scenario 5 ($f_d = f_d - 0.01$)	1000	0.49	1500	0.29	500	0.69
Experiment 2, Scenario 1 (observed PPFD, mean time-varying f_d)	1000	0.5	1500	0.5	500	0.5
Experiment 2, Scenario 2 (observed f_d, mean time-varying PPFD)	1000	0.5	1000	0.3	1000	0.7

Experiments and Scenarios	Hypothetical Example: 10:00–10:30 am of June 11					
	2004		2005		2006	
	PPFD	f_d	PPFD	f_d	PPFD	f_d
Experiment 3, Scenario 1 (Weiss and Norman model)	1000	Weiss and Norman model	1500	Weiss and Norman model	500	Weiss and Norman model
Experiment 3, Scenario 2 (Spitters et al. model)	1000	Spitters et al. model	1500	Spitters et al. model	500	Spitters et al. model

For Experiment (3), we again used the same parameter set as before but combined FöBAAR with one of two models for predicting diffuse fraction: (1) Weiss and Norman (1985)(2) Spitters et al. (1986). We assessed how accurately these models predict diffuse fraction, when errors occur, and how these errors propagate to errors in modeling of NEE and other ecosystem variables.

3. Results

3.1. Model performance with observed diffuse fraction

To establish a benchmark against which we could compare model runs using manipulated diffuse fraction, we first optimized the model to all data constraints using observed diffuse fraction (base scenario).

At the annual time step, modeled NEE was consistent with gap-filled NEE for the majority of the years in both training and validation periods (Fig. 1a). During training, the mean absolute error was ≈48 g C m^{-2} yr^{-1}, slightly above the mean annual uncertainty of ≈ ±32 g C $m^{-2}yr^{-1}$. FöBAAR captured the interannual patterns of NEE increase and decrease, but overestimated net uptake in 2006 by ≈72 g C m^{-2} yr^{-1} and underestimated net uptake the following year by ≈75 g C m^{-2} yr^{-1}. Surprisingly, the mean absolute error dropped to ≈42 g C m^{-2} yr^{-1} during validation period, on par with the mean annual uncertainty of ≈ ±42 g C m^{-2} yr^{-1}, although the interannual trend of NEE was less closely replicated compared to the training period. Overall, model estimates and their 90% confidence intervals were within the uncertainty bounds of data for six of the ten years (excluding 2006 and 2007 during the training period, 2010 and 2013 during the validation period) with no systematic under- or overestimation of fluxes.

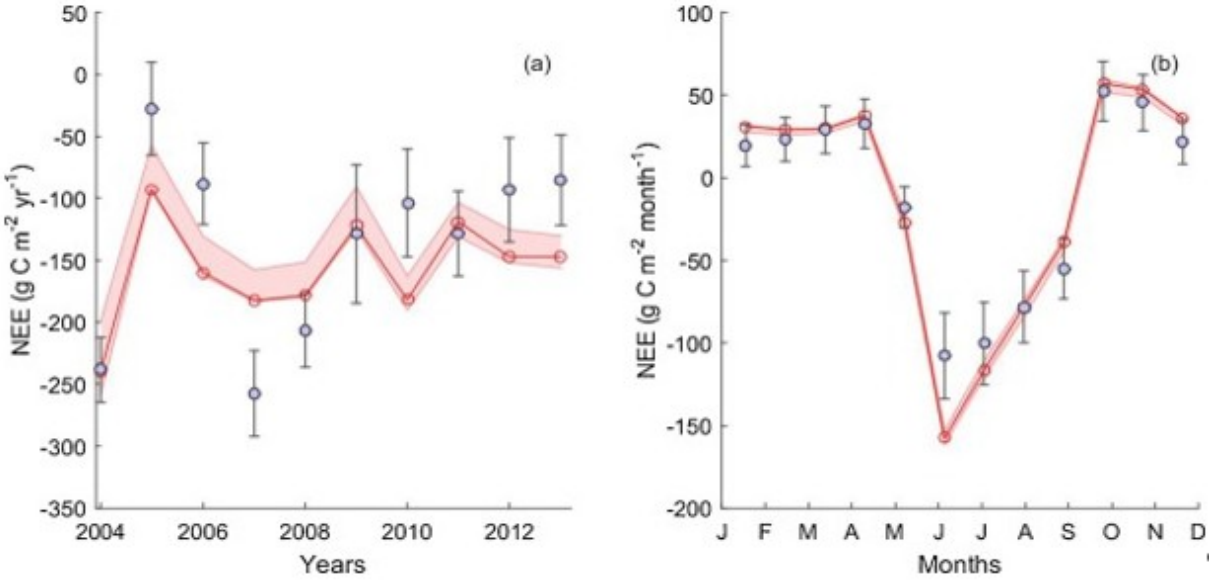

Fig. 1. Modeled (red) and gap-filled (gray) NEE sums at annual (a) and monthly (b) time scales. Points in (b) represent average NEE for the given month during validation period (2009-13). Red shaded bar indicates 90% confidence interval generated using the posterior chi-squared test. Error bars indicate uncertainties of gap-filled sums, which include measurement, gap-filling, and u* uncertainties following the approach of Barr et al. (2013). (For interpretation of the references to colour in this figure legend, the reader is referred to the web version of this article.)

While it is possible for models to replicate annual flux sums without replicating the seasonal cycle, our results indicated fairly accurate modeling of fluxes at the monthly time step. During training period, the mean absolute error for monthly NEE was ≈22 g C m^{-2} $month^{-1}$during the peak productivity season of June, July, and August, and ≈12 g C m^{-2} $month^{-1}$ for rest of the year. These errors remained the same during the validation period, indicating no major shift in model performance. One persistent bias that emerged was the overestimation of net uptake in June; model estimates overshot gap-filled sums by an average of ≈34 g C m^{-2} $month^{-1}$ during validation, compared to mean uncertainty of ≈ ±26 g C $m^{-2}$$month^{-1}$ for June (Fig. 1b).

The model generally yielded a good fit to observations across the various data constraints (Table 4). Errors were low for foliar litterfall and turnover rates of soil pools during both training and validation periods, and also for soil respiration, woody litterfall, and LAI, which had measurements only during training period. Daytime fluxes were not modeled quite as accurately as nighttime fluxes, and annual wood growth not as accurately as annual NEE, but the average NRMSE across all data constraints was below one for both training and validation periods, indicating that key ecosystem processes were represented reasonably well given uncertainties in the data.

Table 4. NRMSEs for each of the data constraints, by diffuse fraction model and time period. These are uncertainty-weighted root mean squared errors calculated using Eq. (18) in Materials and Methods. All model runs shown here used the same optimal parameter set from the base scenario, and differed only in the way in which the direct and diffuse PPFD was prescribed.

	Training Period			**Validation Period**		
	Weiss and Norman	**Spitters et al.**	**Observed**	**Weiss and Norman**	**Spitters et al.**	**Observed**
Nighttime NEE	0.78	0.56	0.63	0.69	0.47	0.55
Daytime NEE	3.05	2.21	2.29	3.58	2.27	2.45
Monthly NEE	0.47	0.34	0.33	0.47	0.27	0.28
Annual NEE	4.45	3.91	1.66	1.33	1.95	0.32
LAI	4.95	0.12	0.48	–	–	–
Foliar litterfall	1.80	2.69	1.41	2.46	0.14	0.21
Woody litterfall	0.01	0.01	0.01	–	–	–
Annual wood growth	7.49	4.82	3.57	5.74	9.12	3.93
Multi-year wood growth	2.85	1.10	0.04	2.67	5.41	0.98
Soil respiration	0.91	0.42	0.50	–	–	–
Litter turnover	0.03	0.02	0.03	0.02	0.02	0.02

	Training Period			Validation Period		
	Weiss and Norman	**Spitters et al.**	**Observed**	**Weiss and Norman**	**Spitters et al.**	**Observed**
SOM 1 turnover (microbial)	0.06	0.06	0.06	0.13	0.13	0.13
SOM 2 turnover (slow)	0.28	0.28	0.28	0.20	0.20	0.20
SOM 3 turnover (passive)	0.09	0.09	0.09	0.07	0.07	0.07
Average NRMSE	**1.94**	**1.19**	**0.81**	**1.58**	**1.82**	**0.83**

3.2. Model sensitivity to diffuse fraction

To assess how modeled GPP responds to changes in diffuse fraction (f_d), we compared FöBAAR runs using the same optimized parameter set but different scenarios of f_d as per Experiment (1).

We observed that modeled GPP was significantly higher when f_d increased from 0 to 1 (Fig. 2b,c) − under the admittedly unrealistic assumption that total PPFD is constant − because the enhanced productivity of shaded leaves far outweighed the reduced productivity of sunlit leaves, due to the saturating relationship between PPFD and photosynthesis. The PPFD on shaded leaves reached a maximum when all light was diffuse, as per Eq. (1) (see Section 2.3.2). Even though PPFD on shaded leaves was above zero when all light was direct because of scattered direct beam, this component was relatively small, and the GPP of shaded leaves was eight to ninefold higher under maximum f_d (Fig. 2a). The GPP of sunlit leaves decreased when f_d changed from 0 to 1 due to the absence of the direct light contribution to PPFD, but this was partially offset by the larger diffuse PPFD. Therefore, the drop in GPP of sunlit leaves was smaller compared to the increase in GPP of shaded leaves, and the overall GPP from both leaf classes more than doubled when f_d increased from 0 to 1 at PPFD of 1100 μ mol m^{-2} s^{-1} or more (Fig. 2b). However, because of saturation in the photosynthetic light response function, canopy GPP did not scale linearly with f_d; prescribing f_d of 0.5 in Scenario (3) resulted in GPP that was greater than the average of GPP under entirely direct and entirely diffuse light (Fig. 2b). For the same reason, the enhancement of canopy GPP with increasing f_d (holding total PPFD constant) was largest when f_d is small.

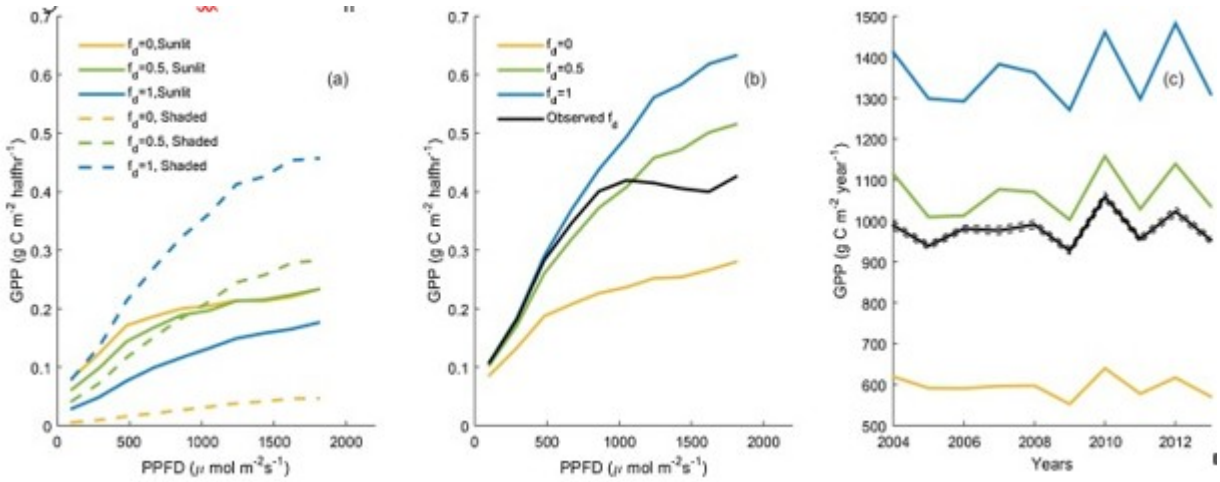

Fig. 2. Mean modeled GPP when diffuse fraction is set at zero (yellow), one-half (green), one (blue), and observed levels (black). GPP is shown for (a) sunlit (solid line) and shaded (dotted line) leaves at half-hourly time step (b) sum of sunlit and shaded leaves at half-hourly time step (c) sum of sunlit and shaded leaves at annual time step. Dashed black line in (c) indicates scenario of ±0.01 change in observed levels of diffuse fraction. Observed levels of diffuse fraction range from 0.10 to 0.99 in (b) and 0.40–0.47 in (c). Only daylight periods in June, July, and August are shown in (a) and (b). (For interpretation of the references to colour in this figure legend, the reader is referred to the web version of this article.)

Accumulated over the course of the growing period, f_d-mediated changes in productivity produced substantial differences in annual GPP. The GPP in Scenario (2) (f_d = 1) was higher than GPP in Scenario (1) (f_d = 0) by ≈760 g C m^{-2} $year^{-1}$, a ≈130% increase (Fig. 2c). The GPP in Scenario (3) (f_d = 0.5) exceeded that in Scenario (1) by an average of ≈470 g C m^{-2} $year^{-1}$, which is ≈62% of the GPP difference between Scenarios (1) and (2). When observed levels of f_d − which ranged from 0.40 to 0.47 annually − were increased and decreased by 0.01 in Scenarios (4) and (5) to assess GPP's sensitivity to small changes in diffuse fraction, the annual GPP increased and decreased by ≈9.2 g C m^{-2} $year^{-1}$, respectively (Fig. 2c). Therefore, a 1 percentage point change in observed percentage of radiation that is diffuse, holding total PPFD constant, produced a ≈0.94% change in annual GPP.

To evaluate how much interannual variability of f_d potentially explains the interannual variability of carbon budgets at our site, we conducted Experiment (2) which examined two additional scenarios: (1) every half-hour of the year is assigned observed PPFD but mean time-varying f_d (2) every half-hour is assigned observed f_d but mean time-varying PPFD.

On average, prescribing observed PPFD and mean time-varying f_d caused much larger deviations in modeled annual NEE compared to prescribing observed f_d and mean time-varying PPFD. Use of mean time-varying f_d produced a mean deviation of ≈48 g C m^{-2} $year^{-1}$ from the annual NEE of the base scenario (Fig. 3). The magnitude of deviation varied substantially across the years, ranging from ≈0.7 g C m^{-2} $year^{-1}$ in 2006 to ≈148 g C m^{-2} $year^{-1}$ in 2004. It is possible that the large deviation in 2004 resulted partly from the use of modeled f_d during May and early June in 2004 (see Section 2.2); the modeled values could be underestimates. However, there were also three other years (2007, 2010, 2012) with deviations greater than 50 g C m^{-2} $year^{-1}$. Use of mean time-varying PPFD, on the other hand, changed modeled annual NEE by an average of only ≈0.4 g C m^{-2} $year^{-1}$ (Fig. 3). This discrepancy indicates that variability of f_d mediates modeled interannual NEE trends more strongly than does variability of total irradiance. The model run using mean time-varying f_d also differed from the run using mean time-varying PPFD in that the former's predicted carbon uptake consistently exceeded estimates under the base scenario. Therefore, while aggregate levels of f_d may be higher in one year than another (annual f_d ranged from ≈0.40–0.47) each year has periods of relatively low f_d, and increasing f_d in these periods enhances annual GPP by more than the loss associated with decreasing f_d in any relatively high f_d periods.

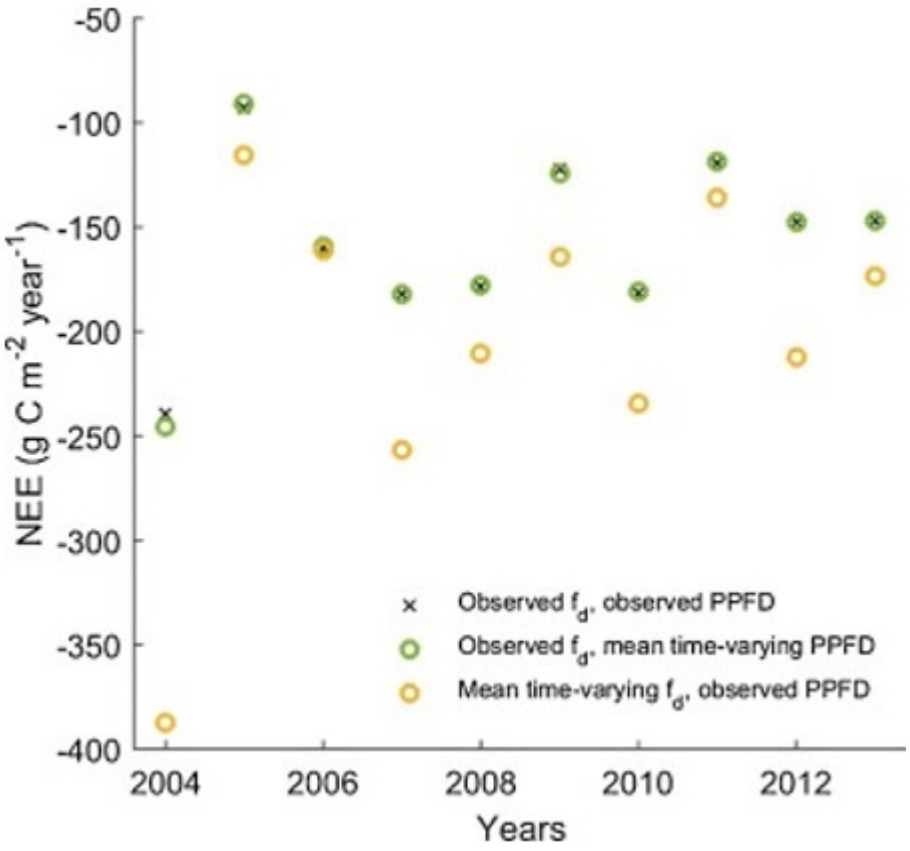

Fig. 3. Annual NEE modeled using observed diffuse fraction and observed photosynthetic photon flux density (PPFD) (black cross); observed diffuse fraction and mean time-varying PPFD (green circle); mean time-varying diffuse fraction and observed PPFD (yellow circle). The three model runs used the same optimal parameter set from the base scenario, and differed only in the way that diffuse fraction and PPFD were prescribed. (For interpretation of the references to colour in this figure legend, the reader is referred to the web version of this article.)

3.3. Modeling diffuse fraction

In Experiment (3), we assessed the performance of two partitioning models that estimate f_d, and analyzed how differences between modeled and measured f_d translate to differences in overall model performance.

The Weiss and Norman (1985) model generally overestimated, and the Spitters et al. (1986)model generally underestimated observed f_d (Fig. 4). The two models, however, displayed similar biases with respect to the solar elevation angle, PPFD, and observed f_d. Overestimation was more pronounced at lower sun angles for the Weiss and Norman model, with the mean f_d error (modeled − observed f_d) peaking at ≈0.26 between 20° and 40° (Fig. 4a), and underestimation increased at higher sun angles for the Spitters et al. model, reaching ≈ −0.6 between 60° and 80° (Fig. 4b). Both models tended to underestimate f_d at higher PPFD. For example, for observed values of f_d between 0.6 and 0.8, the mean f_d error for the Weiss and Norman model changed signs from ≈0.09 at 500 μ mol m^{-2} s^{-1} to ≈ −0.19 at 1500 μ mol m^{-2} s^{-1} (Fig. 4c), while

underestimation of the Spitters et al. model increased by ≈0.17 over the same PPFD range (Fig. 4d). But a difference between the two models was that underestimation of f_d peaked at medium PPFD (≈850 μ mol m^{-2} s^{-1}) for the Spitters et al. model, while it continued increasing with PPFD for the Weiss and Norman model. Finally, both models tended to overestimate f_d when f_d is low, and underestimate f_d when f_d is high (Fig. 4c, d). On average, the Weiss and Norman model predicted f_d more accurately; its RMSE was ≈0.19, compared to ≈0.26 for the Spitters et al. model.

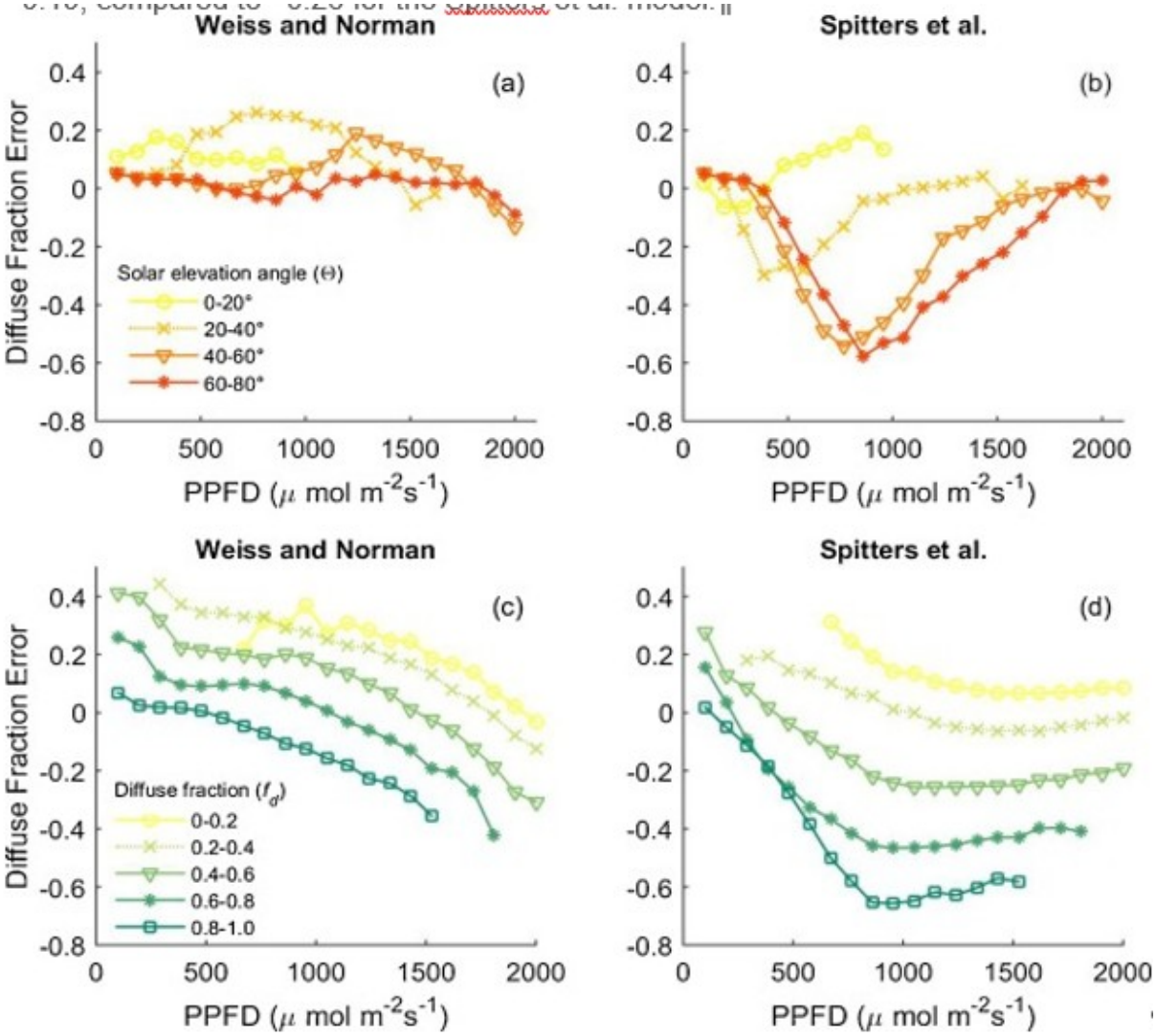

Fig. 4. Diffuse fraction error (modeled minus measured diffuse fraction) averaged by (a) solar elevation angle for Weiss and Norman model (b) solar elevation angle for Spitters et al. model (c) observed diffuse fraction for Weiss and Norman model (d) observed diffuse fraction for Spitters et al. model. Darker lines correspond to higher solar elevation angles in (a) and (b), and higher diffuse fractions in (c) and (d). Only daylight periods in June, July, and August during validation period are shown for each graph.

The biases in estimating f_d propagated to predictions of GPP and therefore, net carbon uptake. Use of the Weiss and Norman model, which generally overestimated f_d, caused overestimation of net carbon uptake (Fig. 5a), while

the opposite was true for the Spitters et al. model (Fig. 5b), which generally underestimated f_d. The relationship between f_d and NEE errors could be confirmed by their matching dependencies on observed f_d. For instance, just as the partitioning models' overestimation of f_d was most severe when observed f_d was below 0.2 (Fig. 4c,d), the same pattern emerged for overestimation of NEE (Fig. 5a,b). The Weiss and Norman model's underestimation of f_d at higher PPFD manifested in less negative NEE errors (i.e. less overestimation of net carbon uptake) starting at PPFD of ≈1250 μ mol m^{-2} s^{-1} (Fig. 5a).

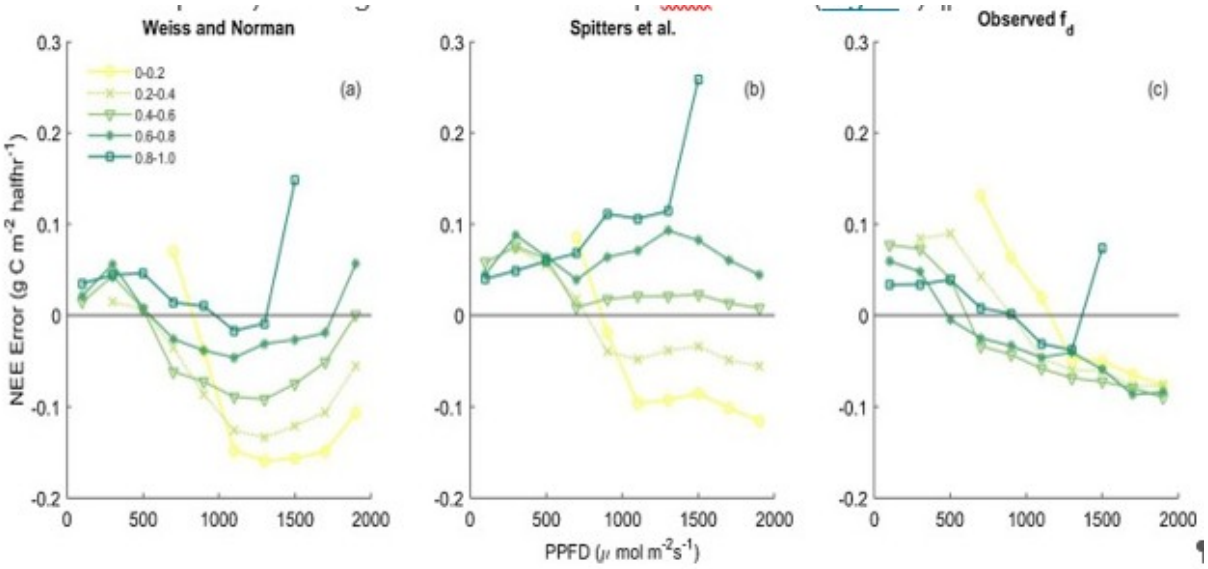

Fig. 5. Half-hourly NEE error (modeled minus measured NEE) averaged by observed diffuse fraction and PPFD for FöBAAR runs using (a) Weiss and Norman model (b) Spitters et al. model (c) observed diffuse fraction. Negative errors represent model overestimation of net carbon uptake (i.e. modeled NEE is more negative than observed NEE), and positive errors represent model underestimation of net carbon uptake. Only daylight periods in June, July, and August during the validation period are shown for each graph.

Overall, FöBAAR's ability to predict NEE declined with the use of modeled f_d, though the decline was more significant with the Weiss and Norman model and at annual scales. At the half-hourly time step, the Weiss and Norman model's tendency to overestimate net carbon uptake, especially during periods of low observed f_d (Fig. 5a) and morning hours (Fig. 6a), increased the NRMSE for daytime NEE by ≈1.13, or ≈46%, during the validation period (Table 4). The Spitters et al. model's underestimations of uptake, however, reduced the NRMSE slightly because FöBAAR had tended to overpredict mid-day uptake when using observed f_d (Fig. 6a). A similar story unfolded at the monthly time step: the Spitters et al. model's lower estimates of net uptake during the growing period had negligible effects on the error because FöBAAR had previously overestimated uptake in those months. However, the Weiss and Norman model's upward bias in June, July, and August raised the mean absolute error for these months by ≈13 g C m^{-2} $month^{-1}$ during validation (Fig. 6b). In addition, mean absolute error in winter and spring (Oct − Mar) increased by ≈4.5 g C m^{-2} $month^{-1}$ with the Weiss and Norman

model because FöBAAR links more productivity with more litterfall and heterotrophic respiration, resulting in underestimation of net carbon uptake outside the growing season. It was at the annual time step that use of either partitioning model caused the most noticeable declines in FöBAAR's performance. During the validation period, modeled net uptake was on average ≈26 g C m^{-2} $year^{-1}$ greater with the Weiss and Norman model, and ≈23 g C m^{-2} $year^{-1}$ lower with the Spitters et al. model, compared to using observed f_d (Fig. 6c). As a result, mean absolute error increased by ≈19 g C m^{-2} $year^{-1}$ with the Weiss and Norman model, and ≈7.8 g C m^{-2} $year^{-1}$ with the Spitters et al. model.

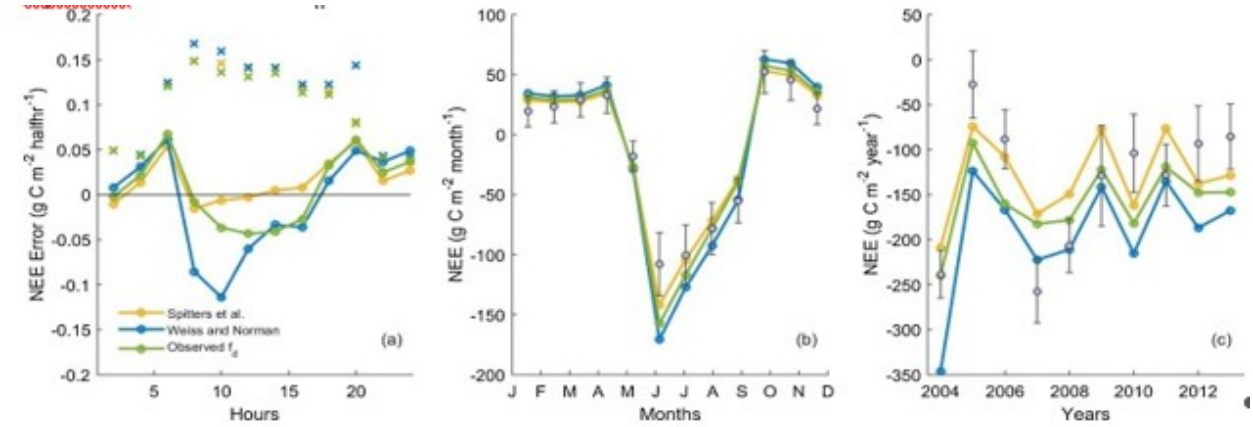

Fig. 6. Comparison of NEE errors and sums among FöBAAR runs using Spitters et al. (yellow), Weiss and Norman model (blue), and observed diffuse fraction (green). (a) NEE error (modeled minus measured NEE) in June, July, August of validation period, averaged in two-hour bins (b) modeled and gap-filled NEE sums at monthly time step during validation period (c) modeled and gap-filled NEE sums at annual time step. The x's in (a) indicate standard deviation of errors for each model run. The error bars in (b) and (c) indicate uncertainties of gap-filled NEE sums, which include measurement, gap-filling, and u* uncertainties following approach of Barr et al. (2013). (For interpretation of the references to colour in this figure legend, the reader is referred to the web version of this article.)

Biased estimates of GPP caused by f_d modeling errors also increased model-data mismatch on annual ancillary constraints (Table 4). Annual wood growth, LAI, and foliar litterfall increased with the Weiss and Norman model because enhanced productivity results in more wood and foliage. Litterfall increase, in turn, stimulated litter decomposition and soil respiration. The opposite cascade of effects occurred when the Spitters et al. model underestimated GPP. The average NRMSE during validation period increased significantly with use of either model (columns 5 and 6, last row of Table 4), mainly due to biased predictions of wood growth.

4. Discussion

By optimizing a forest carbon cycle model to multiple data constraints and prescribing different scenarios of diffuse fraction, we have assessed how the modeling of enhanced photosynthesis under diffuse light affects annual GPP and other ecosystem carbon fluxes.

4.1. Advantages of diffuse light

In the Norman sun-shade canopy model, the distribution of PPFD between leaf layers is more balanced under diffuse light because diffuse PPFD equally contributes to PPFD on shaded and sunlit leaves (in absolute terms), whereas direct PPFD predominantly strikes sunlit leaves. Since leaf photosynthesis becomes saturated at higher light intensities, increasing diffuse fraction, which effectively reallocates PPFD on sunlit leaves bearing the higher radiation load to shaded leaves, enhances overall canopy productivity. We observed in Experiment (1) that when diffuse fraction increases from zero to one, the net gain in annual GPP across both leaf layers is ≈130% (Fig. 2c). Such dramatic variation in diffuse fraction without corresponding changes in PPFD is of course unrealistic, but GPP responses to a 0.01 change in observed values of diffuse fraction, holding total PPFD constant, were ≈9.2 g C m^{-2} $year^{-1}$ (Fig. 2c).

We found that the sensitivity of GPP to changes in diffuse fraction depends on both total irradiance and diffuse fraction. The increase in GPP associated with a given increase in diffuse fraction grew with total irradiance (Fig. 2b) because more severe photosynthetic saturation at higher PPFD was averted. A marginal increase in diffuse fraction also produced greater GPP gains when the diffuse fraction is relatively low, due to photosynthetic saturation. At lower diffuse fraction, the drop in GPP of sunlit leaves associated with an increase in diffuse fraction is smaller because PPFD on sunlit leaves is already abundant, while the concurrent increase in GPP of shaded leaves is larger since PPFD on shaded leaves is minimal. As a result, an increase in diffuse fraction from 0 to 0.5 accounted for ≈62%, rather than 50%, of the GPP gained when diffuse fraction increased from 0 to 1. This non-linear relationship between GPP and diffuse fraction suggests that the moderately high diffuse fraction at which GPP often peaks in forest ecosystems (Alton et al., 2007; Knohl and Baldocchi, 2008; Oliphant et al., 2011; Zhang et al., 2010) likely represents the point where LUE gains have diminished to the extent that they are outweighed by the effect of irradiance reductions with any further increases in diffuse fraction.

Our estimates of GPP changes with diffuse fraction depend to an extent on the parameter values and structure of the canopy model. Knohl and Baldocchi (2008) show, for instance, that while the choice of leaf inclination angle has modest impact on the diffuse light effect, higher scattering coefficients reduce the diffuse light effect because the canopy produces more diffuse radiation of its own and is thus less sensitive to incident diffuse radiation above the canopy. Our estimate of the diffuse light effect is also conservative in that the canopy model does not account for potential changes in leaf temperature and VPD that may accompany changes in PPFD distribution. For example, allowing sunlit leaves to be cooler under higher diffuse fraction would likely enhance diffuse light’s contribution to net carbon uptake by increasing the sunlit leaves’ photosynthesis when air temperature exceeds the optimum (Steiner and Chameides, 2005), reducing their respiration, and/or increasing their stomatal conductance by reducing VPD.

4.2. Modeling diffuse fraction

Given that the ratio of diffuse to direct light is correlated with observable environmental factors, including the solar elevation angle, cloud cover, and global irradiance, information about these variables should aid in modeling diffuse fraction. However, our evaluation of radiation partitioning models from Weiss and Norman (1985) and Spitters et al. (1986) is consistent with previous studies that find non-trivial errors in a range of diffuse fraction models (Badescu et al., 2013; Batlles et al., 2000; Dervishi and Mahdavi, 2012; Noorian et al., 2008). We also observed that the model estimates of diffuse fraction are consistently biased, and this bias is correlated with input variables.

In Experiment (3), the Weiss and Norman model predominantly overestimated diffuse fraction at our site, while the Spitters et al. model predominantly underestimated it. Spatial variability of the relationship between diffuse fraction and predictor variables has been well-documented (Boland et al., 2001; Oliveira et al., 2002; Soler, 1990) so site-specific factors could explain some of this baseline bias. However, the biases of both models were correlated with solar elevation angle, total PPFD, and observed diffuse fraction in similar ways, suggesting that flawed model inferences of cloudiness play a role. The likelihood of underestimating diffuse fraction increased with solar elevation angle, PPFD, and observed diffuse fraction, which correspond to hazy mid-day periods with medium to high irradiance (Fig. 4). This bias pattern is consistent with limitations of the model structures, which at high sun angles, infer overcast conditions from less global radiation and clear conditions from more global radiation. Observations at our study site indicate that diffuse fraction can be highly variable even when other environmental factors are similiar; for example, one standard deviation of observed diffuse fraction when PPFD ranges from 1200 to 1300 μ mol m^{-2} s^{-1}, and sun angle from 60−70° is ≈0.15. In such conditions, both partitioning models often predicted in the lower range of distributed diffuse fraction values.

Improving the accuracy of the two partitioning models would likely entail reducing both parameter and model structure errors. At study sites where measurements of diffuse fraction are available, a systematic approach to reducing parameter errors would be model-data fusion; the parameters could be optimized to achieve the best fit to observed diffuse fraction. The optimization could account for spatially varying environmental controls on diffuse fraction. However, model-data fusion alone has been found to produce only modest improvements in various partitioning models (Dervishi and Mahdavi, 2012), and additional specification of cloud amount and type, and how these influence diffuse fraction in different ways is likely necessary in the model structure. Incorporating additional predictor variables such as sunshine fraction (Elminir, 2007; Ulgen and Hepbasli, 2009) and using artificial neural network models (Jiang, 2008; Khatib et al., 2012) have also shown some promise. Greater availability of direct and diffuse PPFD

measurements across different ecosystems and latitudes will help validate these emerging model structures.

4.3. Impact of diffuse fraction errors

Previous studies have demonstrated, through examining the empirical relationship between diffuse fraction and ecosystem productivity, that distinction of photosynthesis under direct and diffuse light matters for modeling of the terrestrial carbon balance (Gu et al., 2003; Knohl and Baldocchi, 2008; Mercado et al., 2009; Niyogi et al., 2004). By prescribing various scenarios of diffuse fraction and measuring changes in model outputs and performance, we assessed the extent to which errors in diffuse fraction can propagate to errors in modeling NEE and other carbon cycle components.

In Experiment (2), prescribing mean time-varying diffuse fraction and observed PPFD caused larger and more directional deviations in modeled annual NEE, compared to prescribing mean time-varying PPFD and observed diffuse fraction. The difference in magnitude of NEE shifts was significant: mean time-varying diffuse fraction produced a mean shift of $\approx$48 g C m^{-2} $year^{-1}$ − about two-thirds the standard deviation of annual gap-filled NEE ($\approx$74 g C m^{-2} $year^{-1}$) − while mean time-varying PPFD produced a mean shift of only $\approx$0.4 g C m^{-2} $year^{-1}$ (Fig. 3). Therefore, the direct and diffuse composition of irradiance in a given year relative to other years has stronger influence on carbon uptake during that year, compared to relative levels of total irradiance. Furthermore, the model run using mean time-varying diffuse fraction predicted higher carbon uptake relative to the base scenario, even in years with higher than average diffuse fraction, because periods of relatively low diffuse fraction in each year experienced LUE gains. This result points to the carbon cycling importance of interannual variation in not only the aggregate ratio of diffuse to global PPFD, but also the within-year distribution of diffuse PPFD.

When diffuse fraction partitioned using models was prescribed to FöBAAR in Experiment (3), it became apparent that errors in diffuse fraction cause errors in NEE by affecting estimates of both GPP and RE. At the half-hourly time step, the pattern of biases in modeled daytime NEE mirrored that for modeled diffuse fraction: use of the Weiss and Norman model, for instance, led to severe overestimation of net uptake during early morning (Fig. 6a) and periods of low observed diffuse fraction (Fig. 5b), the same conditions under which diffuse fraction is overestimated (Fig. 4a,c). Accumulated over the year, these overestimations on average led to a $\approx$12% increase in annual GPP relative to the base scenario. Annual RE, on average, also increased $\approx$11% with the Weiss and Norman model because GPP gains resulted in larger carbon allocations to root and foliage, and therefore increases in root respiration and litter decomposition. For the Spitters et al. model, which underestimated diffuse fraction, the opposite effects occurred:

photosynthesis decreased, reducing carbon allocations to root and foliage and therefore respiration.

Only the Weiss and Norman model was associated with noticeable declines in FöBAAR's performance at sub-annual scales, but errors for annual NEE increased with use of either partitioning model. The discrepancy in sub-annual performance of the two partitioning models arose because the Weiss and Norman model's upward bias on diffuse fraction estimates amplified FöBAAR's slight tendency to overestimate productivity during the growing period, while the Spitters et al. model's downward bias mitigated that tendency. But at the annual scale, high-frequency biases of both models accumulated to produce significant directional changes, which inevitably translated into larger errors because FöBAAR had not persistently over- or underestimated annual NEE. On average, modeled net uptake during the validation period was ≈26 g C m^{-2} $year^{-1}$ greater with the Weiss and Norman model, and ≈23 g C m^{-2} $year^{-1}$ lower with the Spitters et al. model − major shifts considering the mean annual gap-filled NEE of ≈ –136 g C m^{-2} $year^{-1}$ and its associated uncertainty of ≈ ±37 g C m^{-2} $year^{-1}$.

5. Conclusions

We investigated the contribution of light use efficiency enhancement under diffuse light to forest carbon uptake, as well as the impact of diffuse fraction modeling errors on predictions of the carbon cycle at a temperate deciduous forest. To do so, we combined 10 years of eddy covariance carbon fluxes and direct and diffuse PPFD measurements with a process-based model using a rigorous model-data fusion approach. Our analysis disentangles changes in canopy PPFD distribution from other pathways through which diffuse light conditions influence the carbon budget, and we find that more even PPFD distribution under diffuse light meaningfully enhances primary productivity and also helps explain the interannual variability of net carbon uptake. Furthermore, systematic errors in estimating diffuse fraction—which we show are possible with standard radiation partitioning models—accumulate to bias annual predictions of the forest carbon cycle.

Since modeling of interannual forest carbon budgets requires accurate, high-frequency information about diffuse fraction, the same is likely to be true for predicting decadal or longer trajectories of terrestrial carbon budgets, especially as prevalence and properties of clouds and aerosols show signs of temporally coherent change (Eastman et al., 2011; Norris et al., 2016; Settele et al., 2014). Through impacts on solar radiation, temperature, and precipitation, these atmospheric changes will directly and indirectly influence photosyntheticlight use efficiency of terrestrial vegetation. Developing more accurate models of diffuse fraction will contribute to reducing the uncertainty of terrestrial carbon cycle responses to global climate change.

Acknowledgments

Research at the Bartlett Experimental Forest is supported by the USDA Forest Service’s Northern Research Station. We acknowledge additional support from the National Science Foundation [grant number DEB-1114804], and from the Northeastern States Research Cooperative. TFK was supported by the Director, Office of Science, Office of Biological and Environmental Research of the US Department of Energy [contract number DE-AC02-05CH11231] as part of the RGCM BGC-Climate Feedbacks SFA.

References

Alton et al., 2007

P.B. Alton, P.R. North, S.O. Los**The impact of diffuse sunlight on canopy light-use efficiency, gross photosynthetic product and net ecosystem exchange in three forest biomes**

Glob. Chang. Biol., 13 (2007), pp. 776-787

Alton, 2008

P.B. Alton**Reduced carbon sequestration in terrestrial ecosystems under overcast skies compared to clear skies**

Agric. For. Meteorol., 148 (2008), pp. 1641-1653

Badescu et al., 2013

V. Badescu, C.A. Gueymard, S. Cheval, C. Oprea, M. Baciu, A. Dumitrescu, F. I acobescu, I.Milos, C. Rada**Accuracy and sensitivity analysis for 54 models of computing hourly diffuse solar irradiation on clear sky**

Theor. Appl. Climatol., 111 (2013), pp. 379-399

Baldocchi and Harley, 1995

D.D. Baldocchi, P.C. Harley**Scaling carbon-dioxide and water-vapor exchange from leaf to canopy in a deciduous forest. 2. model testing and application**

Plant Cell Environ., 18 (1995), pp. 1157-1173

Baldocchi, 1994

D. Baldocchi**An analytical solution for coupled leaf photosynthesis and stomatal conductance models**

Tree Physiol., 14 (1994), pp. 1069-1079

Baldocchi, 1997

D. Baldocchi**Measuring and modelling carbon dioxide and water vapour exchange over a temperate broad-leaved forest during the 1995 summer drought**

Plant Cell Environ., 20 (1997), pp. 1108-1122

Ball et al., 1987

J.T. Ball, I.E. Woodrow, J.A. Berry**A model predicting stomatal conductance and its contribution to the control of photosynthesis under different environmental conditions**

Prog. Photosynth. Res. (1987), pp. 221-224

Barr et al., 2013

A.G. Barr, A.D. Richardson, D.Y. Hollinger, D. Papale, M.A. Arain, T.A. Black, G. Bohrer, D.Dragoni, M.L. Fischer, L. Gu, B.E. Law, H.A. Margolis, J.H. Mccaughey, J.W. Munger, W. Oechel, K.Schaeffer**Use of change-point detection for friction-velocity threshold evaluation in eddy-covariance studies**

Agric. For. Meteorol., 171-172 (2013), pp. 31-45

Barrett et al., 2005

D.J. Barrett, I. Michael J
Hill, L.B. Hutley, J. Beringer, J.H. Xu, G.D. Cook, J.O. Carter, R.J.Williams**Prospects for improving savanna biophysical models by using multiple-constraints model-data assimilation methods**

Aust. J. Bot., 53 (2005), pp. 689-714

Bash et al., 2016

J.O. Bash, K.R. Baker, M.R. Beaver**Evaluation of improved land use and canopy representation in BEIS v3.61 with biogenic VOC measurements in California**

Geosci. Model Dev., 9 (2016), pp. 2191-2207

Batlles et al., 2000

F.J. Batlles, M.A. Rubio, J. Tovar, F.J. Olmo, L. Alados-Arboledas**Empirical modeling of hourly direct irradiance by means of hourly global irradiance**

Energy, 25 (2000), pp. 675-688

Bernacchi et al., 2001

C.J. Bernacchi, E.L. Singsaas, C. Pimentel, A.R. Portis, S.P. Long**Improved temperature response functions for models of Rubisco-limited photosynthesis**

Plant, Cell Environ., 24 (2001), pp. 253-259

Bernier et al., 2008

P. Bernier, P.J. Hanson, P.S. Curtis**Measuring litterfall and branchfall**

C.M. Hoover (Ed.), Field Measurements for Forest Carbon Monitoring: A Landscape-Scale Approach, SpringerNetherlands, Dordrecht (2008), pp. 91-101

Boland et al., 2001

J. Boland, L. Scott, M. Luther**Modelling the diffuse fraction of global solar radiation on a horizontal surface**

Environmetrics, 12 (2001), pp. 103-116

Bonan, 2008

G.B. Bonan**Forests and climate change forcings, feedbacks, and the climate benefits of forests**

Science, 80 (320) (2008), pp. 1444-1449

Boucher et al., 2013

O. Boucher, D. Randall, P. Artaxo, C. Bretherton, G. Feingold, P. Forster, V.-M. Kerminen, Y.Kondo, H. Liao, U. Lohmann, P. Rasch, S.K. Satheesh, S. Sherwoo d, B. Stevens, X.Y. Zhang, X.Y. Zhan**Clouds and aerosols. clim. chang**

2013 Phys. Sci. Basis. Contrib. Work. Gr. I to Fifth Assess. Rep. Intergov. Panel Clim. Chang. (2013), pp. 571-657

Bradford et al., 2010

J.B. Bradford, P. Weishampel, M.L. Smith, R. Kolka, R.A. Birdsey, S.V. Ollinger, M.G. Ryan**Carbon pools and fluxes in small temperate forest landscapes: variability and implications for sampling design**

For. Ecol. Manage., 259 (2010), pp. 1245-1254

Cabrera-Bosquet et al., 2016

L. Cabrera-Bosquet, C. Fournier, N. Brichet, C. Welcker, B. Suard, F. Tardie u**High-throughput estimation of incident light, light interception and radiation-use efficiency of thousands of plants in a phenotyping platform**

New Phytol., 212 (2016), pp. 269-281

Cheng et al., 2015

S.J. Cheng, G. Bohrer, A.L. Steiner, D.Y. Hollinger, A. Suyker, R.P. Phillips, K.J. Nadelhoffer**Variations in the influence of diffuse light on gross primary productivity in temperate ecosystems**

Agric. For. Meteorol., 201 (2015), pp. 98-110

Cheng et al., 2016

S.J. Cheng, A.L. Steiner, D.Y. Hollinger, G. Bohrer, K.J. Nadelhoffer**Using satellite-derived optical thickness to assess the influence of clouds on terrestrial carbon uptake**

J. Geophys. Res. G Biogeosci., 121 (2016), pp. 1747-1761

Choudhury, 2001

B.J. Choudhury**Modeling radiation- and carbon-use efficiencies of maize sorghum, and rice**

Agric. For. Meteorol., 106 (2001), pp. 317-330

Cruse et al., 2015

M.J. Cruse, C.J. Kucharik, J.M. Norman**Using a simple apparatus to measure direct and diffuse photosynthe.tically active radiation at remote locations**

PLoS One (2015), p. 10

De Pury and Farquhar, 1997

D.G.G. De Pury, G.D. Farquhar**Simple scaling of photosynthesis from leaves to canopies without the errors of big-leaf models**

Plant, Cell Environ., 20 (1997), pp. 537-557

Dervishi and Mahdavi, 2012

S. Dervishi, A. Mahdavi**Computing diffuse fraction of global horizontal solar radiation: a model comparison**

Sol. Energy, 86 (2012), pp. 1796-1802

Eastman et al., 2011

R. Eastman, S.G. Warren, C.J. Hahn**Variations in cloud cover and cloud types over the ocean from surface observations, 1954–2008**

J. Clim., 24 (2011), pp. 5914-5934

Elminir, 2007

H.K. Elminir**Experimental and theoretical investigation of diffuse solar radiation: data and models quality tested for Egyptian sites**

Energy, 32 (2007), pp. 73-82

Farquhar and Roderick, 2003

G.D. Farquhar, M.L. Roderick**Atmospheric science. Pinatubo diffuse light, and the carbon cycle**

Science, 299 (2003), pp. 1997-1998

Farquhar et al., 1980

G.D. Farquhar, S. von Caemmerer, J.A. Berry**A biochemical model of photosynthetic CO2 assimilation in leaves of C3 species**

Planta, 149 (1980), pp. 78-90

Fleisher et al., 2015

D.H. Fleisher, A. Dathe, D.J. Timlin, V.R. Reddy**Improving potato drought simulations: assessing water stress factors using a coupled model**

Agric. For. Meteorol., 200 (2015), pp. 144-155

Foken et al., 2012

T. Foken, M. Aubinet, R. Leuning**The Eddy Covariance Method**

Eddy Covariance Springer, Netherlands, Dordrecht (2012), pp. 1-19

Franks et al., 1999

S.W. Franks, K.J. Beven, J.H.C. Gash**Multi-objective conditioning of a simple SVAT model**

Hydrol. Earth Syst. Sci., 3 (1999), pp. 477-489

Goudriaan, 1988

J. Goudriaan**The bare bones of leaf-angle distribution in radiation models for canopy photosynthesis and energy exchange**

Agric. For. Meteorol., 43 (1988), pp. 155-169

Gu et al., 1999

L. Gu, J.D. Fuentes, H.H. Shugart, R.M. Staebler, T.A. Black**Responses of net ecosystem exchanges of carbon dioxide to changes in cloudiness: results from two North American deciduous forests**

J. Geophys. Res. Atmos., 104 (1999), pp. 31421-31434

Gu et al., 2002

L. Gu, D. Baldocchi, S.B. Verma, T.A. Black, T. Vesala, E.M. Falge, P.R. Dowty **Advantages of diffuse radiation for terrestrial ecosystem productivity**

J. Geophys. Res. Atmos., 107 (2002)

(ACL 2-1-ACL 2–23)

Gu et al., 2003

L. Gu, D.D. Baldocchi, S.C. Wofsy, J.W. Munger, J.J. Michalsky, S.P. Urbanski, T .a. Boden**Response of a deciduous forest to the Mount Pinatubo eruption: enhanced photosynthesis**

Science, 299 (2003), pp. 2035-2038

Hastings, 1970

W.K. Hastings**Monte carlo sampling methods using Markov chains and their applications**

Biometrika, 57 (1970), pp. 97-109

Heimann and Reichstein, 2008

M. Heimann, M. Reichstein**Terrestrial ecosystem carbon dynamics and climate feedbacks**

Nature, 451 (2008), pp. 289-292

Hocker and Earley, 1983

H.W. Hocker, D.J. Earley**Biomass and Leaf Area Equations for Northern Forest Species**

New Hampshire Agricultural Experiment Station, University of New Hampshire, Durham, N.H (1983)

Hollinger et al., 1994

D.Y. Hollinger, F.M. Kelliher, J.N. Byers, J.E. Hunt, T.M. McSeveny, P.L. Weir**Carbon dioxide exchange between an undistrubed old-growth temperate forest and the atmosphere**

Ecology, 75 (1994), pp. 134-150

Hollinger et al., 2004

D.Y. Hollinger, J. Aber, B. Dail, E.A. Davidson, S.M. Goltz, H. Hughes, M.Y. Lecl erc, J.T.Lee, A.D. Richardson, C. Rodrigues, N.A. Scott, D. Achuatavarier, J. W alsh**Spatial and temporal variability in forest-atmosphere CO2 exchange**

Glob. Chang. Biol., 10 (2004), pp. 1689-1706

Hollinger, 2008

D.Y. Hollinger**Defining a landscape-scale monitoring tier for the north american carbon program**

C.M. Hoover (Ed.), Field Measurements for Forest Carbon Monitoring: A Landscape-Scale Approach, SpringerNetherlands, Dordrecht (2008), pp. 3-16

Jenkins et al., 2007

J.P. Jenkins, A.D. Richardson, B.H. Braswell, S.V. Ollinger, D.Y. Hollinger, M.L. Smith**Refining light-use efficiency calculations for a deciduous forest canopy using simultaneous tower-based carbon flux and radiometric measurements**

Agric. For. Meteorol., 143 (2007), pp. 64-79

Jiang, 2008

Y. Jiang**Prediction of monthly mean daily diffuse solar radiation using artificial neural networks and comparison with other empirical models**

Energy Policy, 36 (2008), pp. 3833-3837

Kanniah et al., 2012

K.D. Kanniah, J. Beringer, P. North, L. Hutley**Control of atmospheric particles on diffuse radiation and terrestrial plant productivity: a review**

Prog. Phys. Geogr., 36 (2012), pp. 209-237

Keenan et al., 2011

T.F. Keenan, M.S. Carbone, M. Reichstein, A.D. Richardson**The model-data fusion pitfall: assuming certainty in an uncertain world**

Oecologia, 167 (2011), pp. 587-597

Keenan et al., 2012

T.F. Keenan, E. Davidson, A.M. Moffat, W. Munger, A.D. Richardson**Using model-data fusion to interpret past trends, and quantify uncertainties in future projections: of terrestrial ecosystem carbon cycling**

Glob. Chang. Biol., 18 (2012), pp. 2555-2569

Khatib et al., 2012

T. Khatib, A. Mohamed, M. Mahmoud, K. Sopian**An assessment of diffuse solar energy models in terms of estimation accuracy**

Energy Procedia (2012), pp. 2066-2074

Knohl and Baldocchi, 2008

A. Knohl, D.D. Baldocchi**Effects of diffuse radiation on canopy gas exchange processes in a forest ecosystem**

J. Geophys. Res. Biogeosci., 113 (2008), pp. 1-17

Knorr and Kattge, 2005

W. Knorr, J. Kattge**Inversion of terrestrial ecosystem model parameter values against eddy covariance measurements by Monte Carlo sampling**

Glob. Chang. Biol., 11 (2005), pp. 1333-1351

McFarlane et al., 2013

K.J. McFarlane, M.S. Torn, P.J. Hanson, R.C. Porras, C.W. Swanston, M.A. Calla ham, T.P. Guilderson**Comparison of soil organic matter dynamics at five temperate deciduous forests with physical fractionation and radiocarbon measurements**

Biogeochemistry, 112 (2013), pp. 457-476

Mercado et al., 2006

L. Mercado, J. Lloyd, F. Carswell, Y. Malhi, P. Meir, A.D. Nobre**Modelling Amazonian forest eddy covariance data: a comparison of big leaf versus sun/shade models for the C-14 tower at Manaus I. Canopy photosynthesis**

Acta Amaz., 36 (2006), pp. 69-82

Mercado et al., 2009

L.M. Mercado, N. Bellouin, S. Sitch, O. Boucher, C. Huntingford, M. Wild, P.M. Cox**Impact of changes in diffuse radiation on the global land carbon sink**

Nature, 458 (2009), pp. 1014-1017

Metropolis et al., 1953

N. Metropolis, A.W. Rosenbluth, M.N. Rosenbluth, A.H. Teller, E. Teller**Equation of state calculations by fast computing machines**

J. Chem. Phys., 21 (1953), pp. 1087-1092

Min and Wang, 2008

Q. Min, S. Wang**Clouds modulate terrestrial carbon uptake in a midlatitude hardwood forest**

Geophys. Res. Lett., 35 (2008)

Niyogi et al., 2004

D. Niyogi, H.I. Chang, V.K. Saxena, T. Holt, K. Alapaty, F. Booker, F. Chen, K.J. Davis, B.Holben, T. Matsui, T. Meyers, W.C. Oechel, R.A. Pielke, R. Wells, K. Wilson, Y. Xue**Direct observations of the effects of aerosol loading on net ecosystem CO2 exchanges over different landscapes**

Geophys. Res. Lett., 31 (2004), p. L20506

Noorian et al., 2008

A.M. Noorian, I. Moradi, G.A. Kamali**Evaluation of 12 models to estimate hourly diffuse irradiation on inclined surfaces**

Renew. Energy, 33 (2008), pp. 1406-1412

Norman, 1982

J. Norman**Simulation of microclimates**

J.L. Hatfield, I.J. Thomason (Eds.), Biometeorology in Integrated Pest Management, Academic Press, New York (1982), pp. 65-99

Norris et al., 2016

J.R. Norris, R.J. Allen, A.T. Evan, M.D. Zelinka, C.W. O'Dell, S.A. Klein**Evidence for climate change in the satellite cloud record**

Nature, 536 (2016), pp. 72-75

Oliphant et al., 2011

A.J. Oliphant, D. Dragoni, B. Deng, C.S.B. Grimmond, H.P. Schmid, S.L. Scott**The role of sky conditions on gross primary production in a mixed deciduous forest**

Agric. For. Meteorol., 151 (2011), pp. 781-791

Oliveira et al., 2002

A.P. Oliveira, J.F. Escobedo, A.J. Machado, J. Soares**Correlation models of diffuse solar-radiation applied to the city of São Paulo, Brazil**

Appl. Energy, 71 (2002), pp. 59-73

Oliveira et al., 2007

P.H.F. Oliveira, P. Artaxo, C. Pires, S. De
Lucca, A. Procópio, B. Holben, J. Schafer, L.F.Cardoso, S.C. Wofsy, H.R. Rocha **The effects of biomass burning aerosols and clouds on the CO2 flux in Amazonia**

Tellus, Ser. B Chem. Phys. Meteorol., 59 (2007), pp. 338-349

Press et al., 2007

W.H. Press, S.a. Teukolsky, W.T. Vetterling, B.P. Flannery**Numerical Recipes**

(3rd edition), The Art of Scientific Computing Cambridge University Press, Cambridge, U.K (2007)

Reed et al., 2014

D.E. Reed, B.E. Ewers, E. Pendall**Impact of mountain pine beetle induced mortality on forest carbon and water fluxes**

Environ. Res. Lett., 9 (2014), p. 105004

Richardson et al., 2006

A.D. Richardson, D.Y. Hollinger, G.G. Burba, K.J. Davis, L.B. Flanagan, G.G. Katul, J.William
Munger, D.M. Ricciuto, P.C. Stoy, A.E. Suyker, S.B. Verma, S.C. Wofsy**A multi-site analysis of random error in tower-based measurements of carbon and energy fluxes**

Agric. For. Meteorol., 136 (2006), pp. 1-18

Richardson et al., 2010

A.D. Richardson, M. Williams, D.Y. Hollinger, D.J.P. Moore, D.B. Dail, E.A. Davidson, N.A. Scott, R.S. Evans, H. Hughes, J.T. Lee, C. Rodrigues, K. Savage**Estimating parameters of a forest ecosystem C model with measurements of stocks and fluxes as joint constraints**

Oecologia, 164 (2010), pp. 25-40

Rocha et al., 2004

A.V. Rocha, H.B. Su, C.S. Vogel, H.P. Schmid, P.S. Curtis**Photosynthetic and water use efficiency responses to diffuse radiation by an aspen-dominated northern hardwood forest**

For. Sci., 50 (2004), pp. 793-801

Roderick et al., 2001

M.L. Roderick, G.D. Farquhar, S.L. Berry, I.R. Noble**On the direct effect of clouds and atmospheric particles on the productivity and structure of vegetation**

Oecologia, 129 (2001), pp. 21-30

Schurgers et al., 2015

G. Schurgers, F. Lagergren, M. Mölder, A. Lindroth**The importance of micrometeorological variations for photosynthesis and transpiration in a boreal coniferous forest**

Biogeosciences, 12 (2015), pp. 237-256

Settele et al., 2014

J. Settele, R.J. Scholes, R.A. Betts, S. Bunn, P. Leadley, D. Nepstad, J.T. Overp eck, M.A.Toboada**Terrestrial and inland water systems. Clim. Chang**

2014 Impacts, Adapt. Vulnerability. Part A Glob. Sect. Asp. Contrib. Work. Gr. II to Fifth Assess. Rep. Intergov. Panel Clim. Chang (2014), pp. 271-359

Soler, 1990

A. Soler**Dependence on latitude of the relation between the diffuse fraction of solar radiation and the ratio of global-to-extraterrestrial radiation for monthly average daily values**

Sol. Energy, 44 (1990), pp. 297-302

Spitters et al., 1986

C.J.T. Spitters, H.A.J.M. Toussaint, J. Goudriaan**Separating the diffuse and direct component of global radiation and its implications for modeling canopy photosynthesis Part I. Components of incoming radiation**

Agric. For. Meteorol., 38 (1986), pp. 217-229

Steiner and Chameides, 2005

A.L. Steiner, W.L. Chameides**Aerosol-induced thermal effects increase modelled terrestrial photosynthesis and transpiration**

Tellus, Ser. B Chem. Phys. Meteorol., 57 (2005), pp. 404-411

Still et al., 2009

C.J. Still, W.J. Riley, S.C. Biraud, D.C. Noone, N.H. Buenning, J.T. Randerson, M .S. Torn, J.Welker, J.W.C. White, R. Vachon, G.D. Farquhar, J.A. Berry**Influenc e of clouds and diffuse radiation on ecosystem-atmosphere CO 2 and CO18O exchanges**

J. Geophys. Res. Biogeosci., 114 (2009), pp. 1-17

Ulgen and Hepbasli, 2009

K. Ulgen, A. Hepbasli**Diffuse solar radiation estimation models for Turkey’s big cities**

Energy Convers. Manag., 50 (2009), pp. 149-156

Urban et al., 2007

O. Urban, D. Janouš, M. Acosta, R. Czerný, I. Marková, M. Navrátil, M. Pavelka, R. Pokorný, M. Šprtová, R. Zhang, V.R. Špunda, J. Grace, M.V. Marek**Ecophys iological controls over the net ecosystem exchange of mountain spruce stand. Comparison of the response in direct vs. diffuse solar radiation**

Glob. Chang. Biol., 13 (2007), pp. 157-168

Weiss and Norman, 1985

A. Weiss, J.M. Norman**Partitioning solar radiation into direct and diffuse: visible and near-infrared components**

Agric. For. Meteorol., 34 (1985), pp. 205-213

Whittaker et al., 1974

R.H. Whittaker, F.H. Bormann, G.E. Likens, T.G. Siccama**The hubbard brook ecosystem study: forest biomass and production**

Ecol. Monogr., 44 (1974), pp. 233-254

Wild, 2009

M. Wild**Global dimming and brightening: a review**

J. Geophys. Res., 114 (2009), p. D00D16

Wohlfahrt et al., 2008

G. Wohlfahrt, A. Hammerle, A. Haslwanter, M. Bahn, U. Tappeiner, A. Cernusc a**Disentangling leaf area and environmental effects on the response of the net ecosystem CO2 exchange to diffuse radiation**

Geophys. Res. Lett., 35 (2008), p. L16805

Wullschleger, 1993

S.D. Wullschleger**Biochemical limitations to carbon assimilation in C3 plants − a retrospective analysis of the A/Ci curves from 109 species**

J. Exp. Bot., 44 (1993), pp. 907-920

Yanai et al., 2010

R.D. Yanai, J.J. Battles, A.D. Richardson, C.A. Blodgett, D.M. Wood, E.B. Rastet ter**Estimating uncertainty in ecosystem budget calculations**

Ecosystems, 13 (2010), pp. 239-248

Young et al., 1980

H.E. Young, J.H. Ribe, K. Wainwright**Weight tables for tree and shrub species in Maine**

Univ. Maine, Life Sci. Agric. Exp. Stn. Misc. Rep., 230 (1980), p. 84

Zhang et al., 2010

M. Zhang, G.-R. Yu, L.-M. Zhang, X.-M. Sun, X.-F. Wen, S.-J. Han, J.-H. Ya n**Impact of cloudiness on net ecosystem exchange of carbon dioxide in different types of forest ecosystems in China**

Biogeosciences, 7 (2010), pp. 711-722

Zhang et al., 2011

B.C. Zhang, J.J. Cao, Y.F. Bai, S.J. Yang, L. Hu, Z.G. Ning**Effects of cloudiness on carbon dioxide exchange over an irrigated maize cropland in northwestern China**

Biogeosci. Discuss, 8 (2011), pp. 1669-1691